UC Santa Cruz

Title

Interface engineering of phase separation in SrRuO3/SrTiO3 hybrid superlattices

Authors

Cui, Zhangzhang
Zhang, Yingying
Zhai, Xiaofang
et al.

Peer reviewed

Observation of electronic phase separation in chemically ordered SrRuO₃/SrTiO₃ hybrid superlattices

Zhangzhang Cui,[1,2,*] Xiaofang Zhai,[3] Hanghui Chen,[4] Yi-De Chuang,[5] Jinghua Guo,[5] Zhengping Fu,[1,2] Yalin Lu[1,2,†]

[1]*Hefei National Laboratory for Physical Sciences at the Microscale, and Department of Materials Science and Engineering, University of Science and Technology of China, Hefei, Anhui 230026, China*

[2]*Anhui Laboratory of Advanced Photon Science and Technology, University of Science and Technology of China, Hefei, Anhui 230026, China*

[3]*School of Physical Science and Technology, ShanghaiTech University, Shanghai 201210, China*

[4]*NYU-ECNU Institute of Physics, NYU Shanghai, Shanghai 200122, China*

[5]*Advanced Light Source, Lawrence Berkeley National Laboratory, Berkeley, CA 94720, USA*

Corresponding authors: *zzcui@ustc.edu.cn, †yllu@ustc.edu.cn

ABSTRACT

Most of the observed electronic phase separation (EPS) phenomena in complex oxides occur in systems with chemical doping, and theories have established the strong correlation between EPS and chemical-doping induced quenched disorder. Recent experiments on fabricated oxide superlattices with exclusion of chemical disorder also confirmed that the EPS disappears in the clean systems. Thus far, the existence of EPS in strongly correlated oxides without the presence of chemical doping or chemical disorder has not been proved. Here, we have built fully chemically ordered hybrid superlattices using prototypical $SrRuO_3$ and $SrTiO_3$ perovskite oxides. Contrary to previous theoretical and experimental results, we observe an EPS of two magnetic phases with perpendicular and cubic magnetic anisotropies, indicating the coexisting metallic and insulating phases in the superlattices. Our results provide an alternative pathway other than the chemical doping to introduce EPS in correlated oxides and strongly suggest that EPS can exist in clean systems without the need of chemical disorder.

Electronic phase separation (EPS) in complex oxides is often manifested by the competition between multiple phases with distinct electronic/magnetic properties [1]. This phenomenon is most prominent in superconducting cuprates and colossal magnetoresistance manganites which typically show the coexistence of metallic and insulating phases on the micron to nanometer length scales [2,3]. In most cases, EPS phenomena are induced by chemical doping through ionic replacements, interstitials, or vacancies in the parent compounds [2-5]. Occasionally, EPS appears in some oxides with no apparent chemical doping, such as $CaFe_3O_5$ and $LuFe_2O_4$; however, cation nonstoichiometry still exists in these oxides [6,7] such that they can be viewed as solid solutions of Fe^{2+} and Fe^{3+}. The chemical dopants inevitably distribute randomly in the lattice, leading to a quenched disorder, and the role of such randomness in phase transition has been one of the main research subjects in condensed matter physics [8,9].

The effects of chemical doping and chemical disorder on EPS in strongly correlated oxides have been extensively studied. In particular, oxygen doping is an indispensable way for inducing the EPS with coexisting superconducting and antiferromagnetic insulating phases in La_2CuO_4 because oxygen dopants not only provide extra charges, the segregation of excess oxygen also helps compensate the long range Coulomb repulsion [2,10]. Similar phenomenon also occurs at the interface of $LaAlO_3/SrTiO_3$ heterostructures where the coexistence of superconductivity and magnetic orders has been reported [11-14]. The selective occupancy of Ti d orbitals at the interface arising from the presence and the non-uniform distribution of oxygen vacancies is believed to be the origin of the EPS [15]. As for the colossal magnetoresistance systems where the ferromagnetic metallic and charge-ordered insulating phases coexist, the chemical dopants modify the Mn-O-Mn bond angle and subsequently tune the bandwidth. The disorder of the dopants leads to a random electron hoping between nearby Mn ions as well as a random exchange interaction between the localized spins [3,16], and theories have predicted that the EPS in manganites would be suppressed if fully chemically ordered structures could be achieved [17-20]. Remarkably, this

prediction was confirmed in recent experiments in which tricolor manganite superlattices (SLs) were fabricated using a layer-by-layer growth technique to exclude chemical disordering [21,22].

Thus far, the existence of EPS in strongly correlated oxides without the presence of chemical doping or chemical disorder has not been proved. This new EPS has far-reaching scientific and technological implications, for example, reducing the power consumption in colossal magnetoresitive devices due to less electronic scattering by the disorders [22], and achieving an intrinsic coexistence of superconductivity and magnetism on the same electrons [23]. In this work, we design hybrid SLs (see schematic illustration in Fig. 1(a)) through a layer-by-layer growth of the prototypical $SrRuO_3$ (SRO) and $SrTiO_3$ (STO) perovskite oxides. We observe an EPS with two magnetic phases that have perpendicular and cubic magnetic anisotropies (MAs), respectively. In addition, we show that this phenomenon implies the coexisting metallic and insulating phases caused by the non-uniform distribution of the metal-oxygen bond angles. Our work provides an alternative methodology rather than the chemical doping to introduce EPS in complex oxides. More significantly, it gives a strong evidence that EPS can exist in properly designed oxide SLs with full chemical ordering.

The hybrid SLs were epitaxially grown on (001)-oriented STO substrates using pulsed laser deposition (PLD) assisted by the in situ monitoring of reflective high-energy electron diffraction (RHEED) patterns. Specifically, $(SRO)_1/(STO)_1/(SRO)_1/(STO)_3$ (referred to as 1/1/1/3) is the combination of $(SRO)_1(STO)_1$ (1/1) and $(SRO)_1/(STO)_3$ (1/3) SLs as schematically illustrated in Fig. 1(a). Similarly, $(SRO)_1/(STO)_2/(SRO)_1/(STO)_3$ (referred to as 1/2/1/3) is the combination of $(SRO)_1/(STO)_2$ (1/2) and 1/3 SLs. As seen in Fig. 1(b), both the growth of SRO and STO layers exhibits clear RHEED intensity oscillations, displaying an excellent layer-by-layer epitaxy and precise single-unit-cell level control. The total repetition of the supercells is 25 (or 50 SRO monolayers) for both SLs. The x-ray diffraction (XRD) ω-2θ scans of the SLs are shown in Fig. 1(c) and Supplemental Material Fig. S1 [24]. The SLs exhibit

sharp diffraction peaks corresponding to the supercell structures as designed. The average out-of-plane lattice constant of a single perovskite layer in the SLs is calculated to be ~3.92 Å. The reciprocal space mappings (RSMs) (Fig. 1(d) and Supplemental Material Fig. S1 [24]) around the (2 0 4), (-2 0 4), (0 2 4), and (0 -2 4) reflections of STO substrates exhibit the same out-of-plane lattice constants, suggesting that the SL is coherently strained and has tetragonal structure. The 1/1/1/3 SL also has a smooth surface as evidenced by the clear step terraces in the atomic force microscope (AFM) image (Fig. 1(e)). All these characterizations demonstrate the high quality of our SL samples.
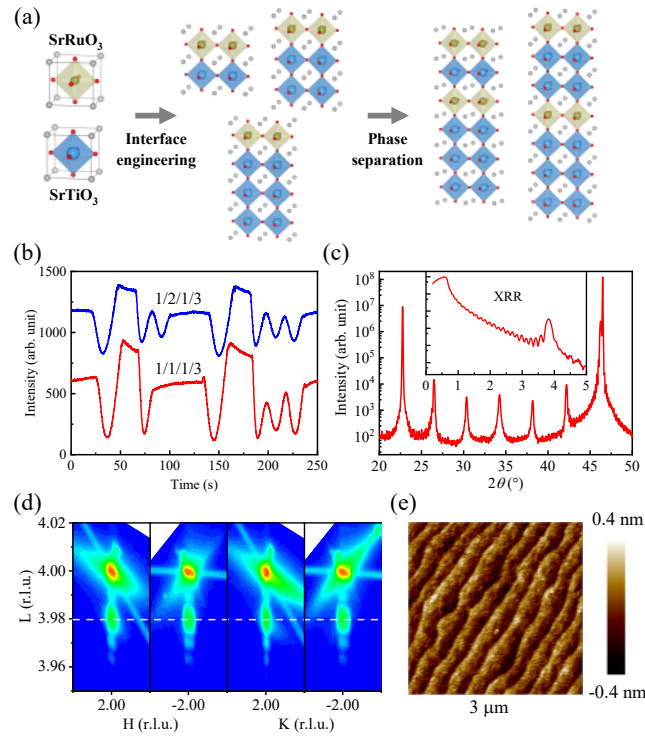

FIG. 1. (a) Schematics of the design of hybrid SLs using the perovskite blocks of pseudo-cubit SRO and STO unit cells. (b) RHEED intensity oscillations of 1/1/1/3 and 1/2/1/3 SLs. (c) XRD ω-2θ scans of 1/1/1/3 SL. The inset shows the x-ray reflectivity (XRR) profile. (d) RSM and (e) AFM images of 1/1/1/3 SL.

Anisotropic magnetoresistance (AMR) is a magneto-transport counterpart of magnetocrystalline anisotropy energy (MAE) which has been widely utilized to investigate the magnetic anisotropy (MA) of magnetic materials [25-28]. The normal AMR effect is caused by the spin-orbit coupling (SOC) that mixes spin-up and spin-down states [29-31] and the resistance simply depends on the angle between the magnetization and the electric current, hence a twofold cosine dependence of the AMR is expected [29]. The MAE can also give rise to a remarkable magnetoresistance that depends on the spin orientations with respect to the crystalline axes, which is caused by the spin-dependent scattering of transport electrons [25,26,32]. Figure 2 shows the AMR of 1/1/1/3 and 1/2/1/3 SLs measured over a broad temperature (T) range. The AMR measurement geometry is schematically shown in Supplemental Material Fig. S2 [24]. For convenience, the pseudo-cubic indices of the SLs are used throughout the article. In Figs. 2(a) and 2(b), the magnetic field (H) of 9 T is rotated in the (001) plane and the electric current (I) is driven along the [110] direction. The 9 T magnetic field is large enough to fully align the electron spins with the field. It can be clearly seen in these figures that the AMRs of both SLs show a fourfold symmetry at $T = 5$ K – 30 K. This fourfold symmetry cannot arise from the normal AMR effort and must be attributed to the MAE symmetry of the SLs.

Figs. 2(c) and 2(d) are the AMRs of 1/1/1/3 and 1/2/1/3 SLs in which the $H = 9$ T field is rotated in the (100) plane and I is driven along the [100] direction. In this measurement geometry, H is always perpendicular to I so that the normal AMR effect is excluded and only the magnetocrystalline component of the AMR is detected. Obviously, the AMRs of both SLs do not show the standard fourfold symmetry. For the 1/1/1/3 SL, at $T = 5$ K and 10 K, an additional AMR with a twofold symmetry overlaps with the fourfold AMR. With increasing temperature, the fourfold AMR gradually diminishes such that at $T = 20$ K and 30 K, the AMR has a nearly standard twofold symmetry. Similarly, for the 1/2/1/3 SL, the AMR at $T = 5$ K is in a fourfold symmetry while with increasing temperature, an additional twofold AMR appears.

6

As a comparison, the AMRs of 1/1 and 1/3 SLs are also measured (see Supplemental Material Fig. S3 [24]) and the pure twofold and fourfold AMRs are observed, respectively. This suggests that the overlapping of twofold and fourfold AMRs is unique to the 1/1/1/3 and 1/2/1/3 SLs.
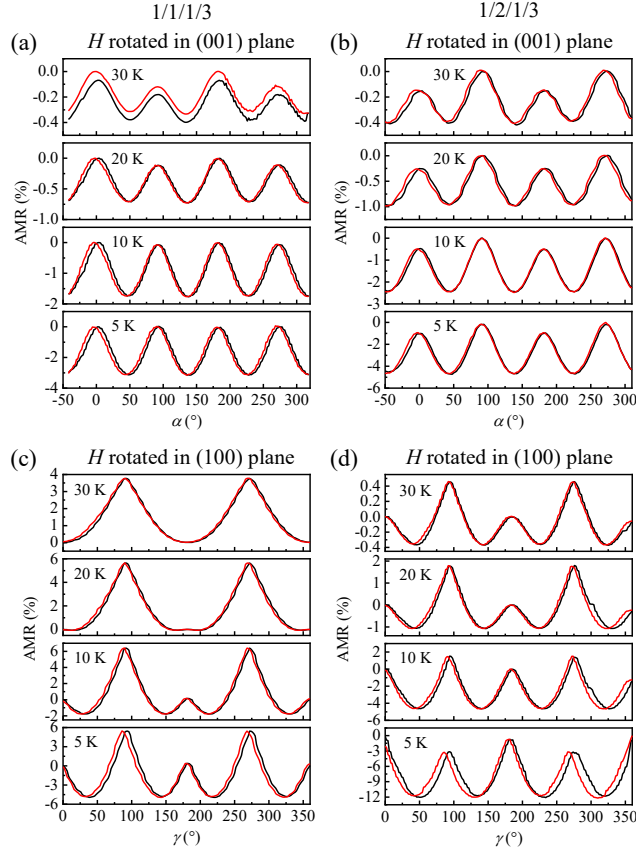

FIG. 2. AMRs of (a) 1/1/1/3 and (b) 1/2/1/3 SLs measured at $T = 5$ K, 10 K, 20 K, and 30 K with H rotated in the (001) plane. The measurements were performed by sweeping H from -45° to 315° (black curves), and then back to -45° (red curves). The electric current is driven along the [110] direction. α is the angle between H and the [110] direction. AMRs of (c) 1/1/1/3 and (d) 1/2/1/3 SLs measured at $T = 5$ K, 10 K, 20 K, and 30 K with H rotated in the (100) plane. The measurements were performed by sweeping H from 0° to 360° (black curves), and then back to 0° (red curves). The electric current is driven along the [100] direction (crystalline a-axis), always perpendicular to H. γ is the angle between H and the [001] direction (crystalline c-axis).

The fourfold AMR observed in both the (001) and (100) planes suggests a cubic MA with eightfold [111] easy axes and the twofold AMR observed in the (100) plane can be attributed to a perpendicular MA with [001] easy axis [33]. Nevertheless, a twofold AMR could also arise from the anisotropic suppression of weak localization in two-dimensional systems in the absence of spin-orbit-coupled scatters or magnetism. This effect predicts a negative magnetoresistance that is largest when H is perpendicular to the film surface [34,35]. To further confirm the origin of the AMR, we examine the magnetic properties of the SLs using a superconducting quantum interference device (SQUID) magnetometer. Figs. 3(a) and 3(b) show the H dependent magnetizations (M) of 1/1/1/3 and 1/2/1/3 SLs measured along the [001] and [111] directions at $T = 5$ K and 30 K. Both SLs show clear magnetic orders with saturation magnetizations over 0.3 μ_B/Ru and saturation fields less than 5 T at $T = 5$ K. The Curie temperatures (T_C) are around 60 K for both SLs (see Supplemental Material Fig. S4 [24]). For the 1/1/1/3 SL, the [001] direction is closer to the magnetic easy axis whereas for the 1/2/1/3 SL, the [111] direction is closer to the easy axis. These observations are qualitatively in agreement with the AMR data considering that the twofold AMR is more prominent in the 1/1/1/3 SL. Moreover, the twofold AMR associated with weak localization is only prominent at temperatures above T_C, as confirmed by the AMR measurement of 1/3 SL at $T = 100$ K and 150 K (see Supplemental Material Fig. S5 [24]). Below T_C, the weak localization contributions would be strongly suppressed due to the existence of magnetic ordering [34]. Generally, it can be concluded from the combined AMR and SQUID measurements that the 1/1/1/3 and 1/2/1/3 hybrid SLs exhibit a coexistence of perpendicular and cubic MAs while the 1/1 and 1/3 SLs show the pure perpendicular and cubic MAs, respectively.

To elucidate the origin of the coexistence of perpendicular and cubic MAs, we measure the resistivity (ρ) and Hall coefficients (R_H) of 1/1, 1/1/1/3, 1/2/1/3, and 1/3 SLs, and the results are shown in Figs. 3(c)

and 3(d). R_H is obtained by fitting the linear slope of the Hall resistance of the SLs (see Supplemental Material Fig. S6 [24]). For the 1/1 SL, the resistivity decreases with increasing temperature but above $T \approx$ 120 K, it shows a mild increase. The R_H is negative and shows weak temperature dependence, indicating a well-defined metallic behavior. With the insertion of STO layers, the resistivity gradually increases and the 1/1/1/3, 1/2/1/3, and 1/3 SLs all show insulating behaviors. In addition, the R_H of 1/3 SL increases sharply and is positive below $T \approx 20$ K. There is a sign change at higher temperature, which is typical for a p-type semiconductor. In contrast, for the 1/1/1/3 and 1/2/1/3 SLs the carriers are primarily electrons while the R_H decreases sharply below approximately the same temperature as that of the 1/3 SL. Furthermore, the temperature dependent evolution of the R_H is in good agreement with that of the AMR. The perpendicular MA is commonly seen in SRO heterostructures with itinerant ferromagnetism [36,37], but the cubic MA in SRO-based heterostructures is very rare and has only been reported in the insulating $(SRO)_1/(STO)_N$ SLs in our previous work [33]. Considering that the 1/1 and 1/3 SLs have only the perpendicular and cubic Mas, respectively, and the EPS usually requires the coexistence of multiple electronic phases, the coexistence of metallic and insulating phases in the 1/1/1/3 and 1/2/1/3 SLs is the natural explanation for the observed AMR and R_H. The temperature dependence of the R_H of 1/1/1/3 and 1/2/1/3 SLs can be explained within the same scenario that the R_H of the metallic phase has weak temperature dependence and an additional p-type semiconducting phase leads to the sharp decrease of the R_H below $T \approx 20$ K.
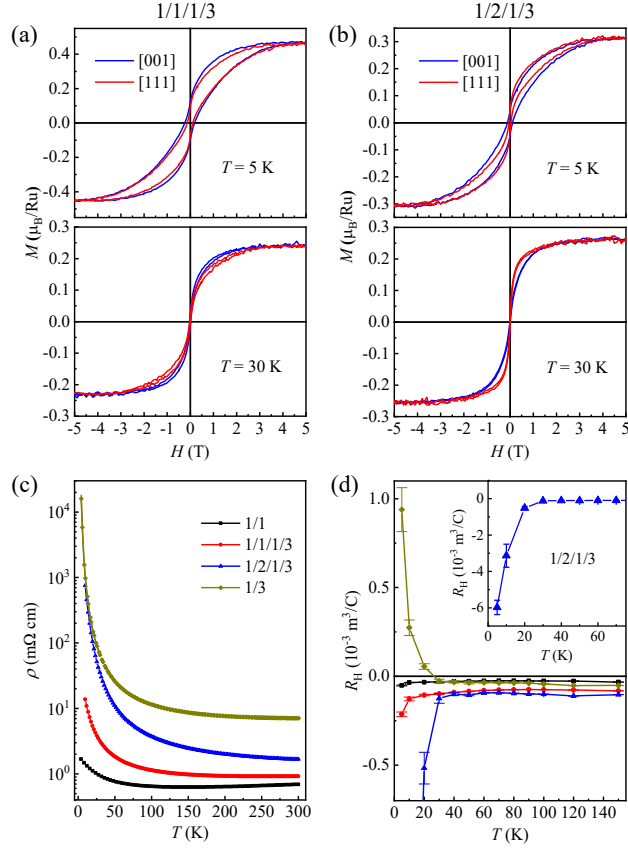
FIG. 3. Magnetic-field dependent magnetizations measured at $T = 5$ K and 30 K along the [001] and [111] directions of (a) 1/1/1/3 and (b) 1/2/1/3 SLs. Temperature dependent (c) resistivity and (d) Hall coefficients of 1/1, 1/1/1/3, 1/2/1/3, and 1/3 SLs. The inset in panel (d) displays the Hall coefficient of the 1/2/1/3 SL at low temperature.

To reveal how the coexistence of metallic and insulating phases emerges, we have performed the detailed atomically resolved cross-sectional aberration-corrected scanning transmission electron microscopy (STEM) measurement on the 1/1/1/3 SL, as shown in Figure 4 and Supplemental Material Fig. S7 [24]. Clear interfaces between SRO and STO are visible in the high-angle annular dark-field (HAADF) STEM images taken at different sites of the SL (see Fig. 4(b) and Supplemental Material Fig. S7(a) [24]), suggesting a good chemical ordering of Ru and Ti atoms across the SL. The positions of the

10

oxygen and metal atom columns are extracted from the annular bright-field (ABF) STEM image (Fig. 4(b)) (see Supplemental Material Fig. S8 [24] for details). We then map the out-of-plane metal-oxygen bond angle $\theta_{M\text{-}O\text{-}M}$ (as indicated in Fig. 4(a), M = Ru and Ti) as a function of oxygen positions, see Fig. 4(c). The statistics of $\theta_{M\text{-}O\text{-}M}$ is summarized in Fig. 4(d). It shows that $\theta_{M\text{-}O\text{-}M}$ has quite a wide dispersion from 156° to 180°. Such a large $\theta_{M\text{-}O\text{-}M}$ dispersion is unusual, unprecedented in most transition-metal perovskite-oxide heterostructures [38-41]. It is known that bulk STO has no out-of-plane oxygen octahedral tilt [42,43], while bulk SRO has a $\theta_{Ru\text{-}O\text{-}Ru}$ around 168° [38]. Compared to the 1/1 and 1/3 SLs, the supercell of the 1/1/1/3 SL is intrinsically asymmetric from the perspective of the SRO layers. Combined with the abrupt discontinuity between the tilts of TiO_6 and RuO_6 octahedra, the interfacial asymmetry will greatly enhance the structural instability. Thus, the non-uniform distribution of $\theta_{M\text{-}O\text{-}M}$ can be the result of the unique asymmetric structures of the hybrid SLs.

The bandwidth and conductivity of the SL are determined by the electron hopping between adjacent SRO monolayers [33]. Moreover, the STO layer thickness and the metal-oxygen bond angle $\theta_{M\text{-}O\text{-}M}$ are the main parameters to control the hopping amplitude. We have shown in our previous first-principles calculation that smaller $\theta_{M\text{-}O\text{-}M}$ will suppress the interlayer electron hopping, leading to a metal-to-insulator transition in the 1/3 SL [33]. Moreover, an earlier calculation reveals a transition from a ferromagnetic metal to an antiferromagnetic insulator triggered by the increased octahedra tilting in the 1/1 SL [41]. Therefore, the EPS of the 1/1/1/3 SL can be related to the non-uniform distribution of the metal-oxygen bond angles that a large $\theta_{M\text{-}O\text{-}M}$ leads to a metallic phase with a perpendicular MA while a small $\theta_{M\text{-}O\text{-}M}$ leads to an insulating phase with a cubic MA (schematically illustrated in Fig. 4(a)). In addition, we have prepared a reference sample of 1/1/1/3 SL that has a larger chemical disorder and its AMR at $T = 5$ K shows a fourfold symmetry (see Supplemental Material Fig. S9 [24]), indicating that increased chemical disorder caused by Ru and Ti intermixing will suppress the EPS in the SL.
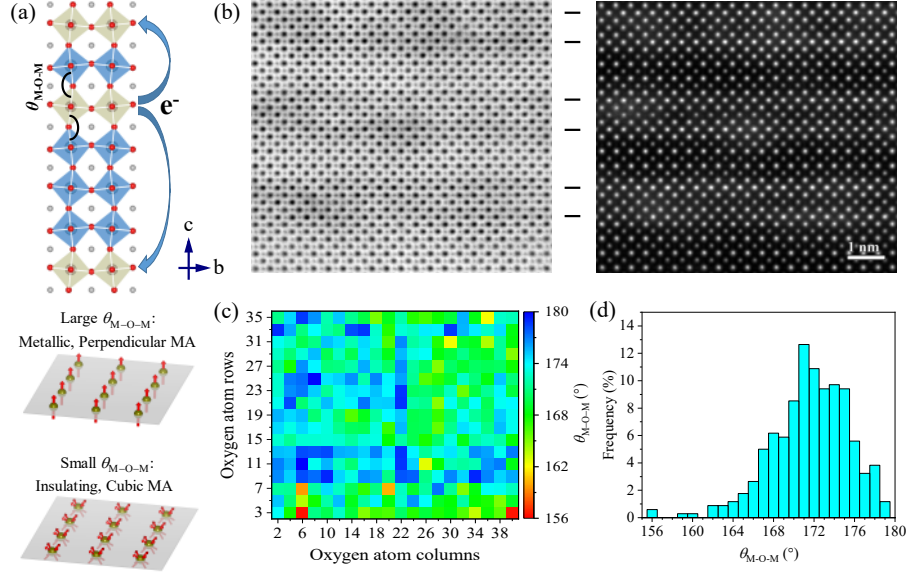
FIG. 4. (a) Schematics of electron hopping between adjacent SRO monolayers (upper panel) and the perpendicular/cubic MA (lower panel). (b) ABF-STEM (left panel) and corresponding HAADF-STEM (right panel) images taken at the same area of 1/1/1/3 SL. The black markers indicate the positions of SRO layers. (c) Map of metal-oxygen bond angle $\theta_{\text{M-O-M}}$ as a function of oxygen positions. (d) Statistical histogram of $\theta_{\text{M-O-M}}$ in a ±0.5° window.

In summary, we have obtained full chemical ordering by fabricating high-quality hybrid SLs of the prototypical SRO and STO perovskite oxides using the layer-by-layer growth technique. In striking contrast to the previous theoretical and experimental studies in transition-metal oxides where chemical disorder is required to seed the EPS, we have demonstrated the presence of EPS into two magnetic phases with perpendicular and cubic MAs in the fully chemically ordered hybrid SLs. We further elucidate that the observed EPS can be attributed to the coexisting metallic and insulating phases arising from the large distribution of the metal-oxygen bond angles. Such EPS share many resemblances with that of the manganites where itinerant ferromagnetism and antiferromagnetism reside in the metallic and insulating phases, respectively. In the SRO/STO hybrid SLs, it can be ascertained that the metallic phase is

ferromagnetic while the magnetic ground state of the insulating phase remains elusive as both ferromagnetism [33] and antiferromagnetism [41,44] were proposed theoretically. The observation of clear hysteresis loops of the anomalous Hall resistivity of the 1/3 SL (Supplemental Material Fig. S6 [24]) indicates that the insulating phase is at least a weak ferromagnet. The identification of these two magnetic phases in the hybrid SLs is challenging, and fortunately they have dramatically different MAs which serves as the signature of the EPS. Our work gives a strong evidence to one of the widely discussed topics in strongly correlated oxides that EPS can exist in clean systems without the need of chemical disorder. Besides, our results provide another methodology other than chemical doping to introduce EPS in complex oxides, which may help to unlock new functionalities.

REFERENCES

[1] S. W. Cheong, P. A. Sharma, N. Hur, Y. Horibe, and C. H. Chen, Physica B **318**, 39 (2002).

[2] E. Sigmund and K. A. Muller, *Phase Separation In Cuprate Superconductors*. (Springer-Verlag, 1993).

[3] E. Dagotto, T. Hotta, and A. Moreo, Phys. Rep. **344**, 1 (2001).

[4] Y. Drees, Z. W. Li, A. Ricci, M. Rotter, W. Schmidt, D. Lamago, O. Sobolev, U. Rutt, O. Gutowski, M. Sprung, A. Piovano, J. P. Castellan, and A. C. Komarek, Nat. Commun. **5**, 5731 (2014).

[5] T. H. Kim, M. Angst, B. Hu, R. Jin, X. G. Zhang, J. F. Wendelken, E. W. Plummer, and A. P. Li, Proc. Natl. Acad. Sci. U.S.A. **107**, 5272 (2010).

[6] K. H. Hong, A. M. Arevalo-Lopez, J. Cumby, C. Ritter, and J. P. Attfield, Nat. Commun. **9**, 2975 (2018).

[7] J. Bourgeois, G. André, S. Petit, J. Robert, M. Poienar, J. Rouquette, E. Elkaïm, M. Hervieu, A. Maignan, C. Martin, and F. Damay, Phys. Rev. B **86**, 024413 (2012).

[8] Y. Imry and S.-k. Ma, Phys. Rev. Lett. **35**, 1399 (1975).

[9] T. Vojta, J. Phys. A: Math. Gen. **39**, R143 (2006).

[10] J. D. Jorgensen, B. Dabrowski, S. Pei, D. G. Hinks, L. Soderholm, B. Morosin, J. E. Schirber, E. L. Venturini, and D. S. Ginley, Phys. Rev. B **38**, 11337 (1988).

[11] L. Li, C. Richter, J. Mannhart, and R. C. Ashoori, Nat. Phys. **7**, 762 (2011).

[12] D. A. Dikin, M. Mehta, C. W. Bark, C. M. Folkman, C. B. Eom, and V. Chandrasekhar, Phys. Rev. Lett. **107**, 056802 (2011).

[13] J. A. Bert, B. Kalisky, C. Bell, M. Kim, Y. Hikita, H. Y. Hwang, and K. A. Moler, Nat. Phys. **7**, 767 (2011).

[14] Ariando, X. Wang, G. Baskaran, Z. Q. Liu, J. Huijben, J. B. Yi, A. Annadi, A. R. Barman, A. Rusydi, S. Dhar, Y. P. Feng, J. Ding, H. Hilgenkamp, and T. Venkatesan, Nat. Commun. **2**, 188 (2011).

[15] V. N. Strocov, A. Chikina, M. Caputo, M. A. Husanu, F. Bisti, D. Bracher, T. Schmitt, F. Miletto Granozio, C. A. F. Vaz, and F. Lechermann, Phys. Rev. Mater. **3**, 106001 (2019).

[16] Y. Tomioka and Y. Tokura, Phys. Rev. B **70**, 014432 (2004).

[17] A. Moreo, M. Mayr, A. Feiguin, S. Yunoki, and E. Dagotto, Phys. Rev. Lett. **84**, 5568 (2000).

[18] J. Burgy, M. Mayr, V. Martin-Mayor, A. Moreo, and E. Dagotto, Phys. Rev. Lett. **87**, 277202 (2001).

[19] C. Şen, G. Alvarez, and E. Dagotto, Phys. Rev. B **70**, 064428 (2004).

[20] C. Sen, G. Alvarez, and E. Dagotto, Phys. Rev. Lett. **98**, 127202 (2007).

[21] T. Miao, L. Deng, W. Yang, J. Ni, C. Zheng, J. Etheridge, S. Wang, H. Liu, H. Lin, Y. Yu, Q. Shi, P. Cai, Y. Zhu, T. Yang, X. Zhang, X. Gao, C. Xi, M. Tian, X. Wu, H. Xiang, E. Dagotto, L. Yin, and J. Shen, Proc. Natl. Acad. Sci. U.S.A **117**, 7090 (2020).

[22] Y. Zhu, K. Du, J. Niu, L. Lin, W. Wei, H. Liu, H. Lin, K. Zhang, T. Yang, Y. Kou, J. Shao, X. Gao, X. Xu, X. Wu, S. Dong, L. Yin, and J. Shen, Nat. Commun. **7**, 11260 (2016).

[23] S. S. Saxena, P. Agarwal, K. Ahilan, F. M. Grosche, R. K. W. Haselwimmer, M. J. Steiner, E. Pugh, I. R. Walker, S. R. Julian, P. Monthoux, G. G. Lonzarich, A. Huxley, I. Sheikin, D. Braithwaite, and J. Flouquet, Nature **406**, 587 (2000).

[24] See Supplemental Material for methods and additional data of structural, magnetic, and transport measurements.

[25] C. Lu, B. Gao, H. Wang, W. Wang, S. Yuan, S. Dong, and J.-M. Liu, Adv. Funct. Mater. **28**, 1706589 (2018).

[26] H. Wang, C. Lu, J. Chen, Y. Liu, S. L. Yuan, S.-W. Cheong, S. Dong, and J.-M. Liu, Nat. Commun. **10**, 2280 (2019).

[27] I. Fina, X. Marti, D. Yi, J. Liu, J. H. Chu, C. Rayan-Serrao, S. Suresha, A. B. Shick, J. Zelezny, T. Jungwirth, J. Fontcuberta, and R. Ramesh, Nat. Commun. **5**, 4671 (2014).

[28] D. Yi, J. Liu, S. L. Hsu, L. Zhang, Y. Choi, J. W. Kim, Z. Chen, J. D. Clarkson, C. R. Serrao, E. Arenholz, P. J. Ryan, H. Xu, R. J. Birgeneau, and R. Ramesh, Proc. Natl. Acad. Sci. U.S.A. **113**, 6397 (2016).

[29] E. D. Dahlberg, K. Riggs, and G. A. Prinz, J. Appl. Phys. **63**, 4270 (1988).

[30] A. P. Malozemoff, Phys. Rev. B **32**, 6080 (1985).

[31] R. Ramos, S. K. Arora, and I. V. Shvets, Phys. Rev. B **78**, 214402 (2008).

[32] P. Li, E. Y. Jiang, and H. L. Bai, Appl. Phys. Lett. **96**, 092502 (2010).

[33] Z. Cui, A. J. Grutter, H. Zhou, H. Cao, Y. Dong, D. A. Gilbert, J. Wang, Y.-S. Liu, J. Ma, Z. Hu, J. Guo, J. Xia, B. J. Kirby, P. Shafer, E. Arenholz, H. Chen, X. Zhai, and Y. Lu, Sci. Adv. **6**, eaay0114 (2020).

[34] R. Scherwitzl, S. Gariglio, M. Gabay, P. Zubko, M. Gibert, and J. M. Triscone, Phys. Rev. Lett. **106**, 246403 (2011).

[35] D. J. Groenendijk, N. Manca, J. de Bruijckere, A. Monteiro, R. Gaudenzi, H. S. J. van der Zant, and A. D. Caviglia, Eur. Phys. J. Plus. **135**, 627 (2020).

[36] W. Lu, P. Yang, W. D. Song, G. M. Chow, and J. S. Chen, Phys. Rev. B **88**, 214115 (2013).

[37] M. Ziese, I. Vrejoiu, and D. Hesse, Phys. Rev. B **81**, 184418 (2010).

[38] D. Kan, R. Aso, R. Sato, M. Haruta, H. Kurata, and Y. Shimakawa, Nat. Mater. **15**, 432 (2016).

[39] Z. Liao, M. Huijben, Z. Zhong, N. Gauquelin, S. Macke, R. J. Green, S. Van Aert, J. Verbeeck, G. Van Tendeloo, K. Held, G. A. Sawatzky, G. Koster, and G. Rijnders, Nat. Mater. **15**, 425 (2016).

[40] M. Saghayezhian, Z. Wang, H. Guo, R. Jin, Y. Zhu, J. Zhang, and E. W. Plummer, Phys. Rev. Res. **1**, 033160 (2019).

[41] M. Gu, Q. Xie, X. Shen, R. Xie, J. Wang, G. Tang, D. Wu, G. P. Zhang, and X. S. Wu, Phys. Rev. Lett. **109**, 157003 (2012).

[42] H. Vogt, Phys. Rev. B **51**, 8046 (1995).

[43] G. Shirane and Y. Yamada, Phys. Rev. **177**, 858 (1969).

[44] S. G. Jeong, T. Min, S. Woo, J. Kim, Y. Q. Zhang, S. W. Cho, J. Son, Y. M. Kim, J. H. Han, S. Park, H. Y. Jeong, H. Ohta, S. Lee, T. W. Noh, J. Lee, and W. S. Choi, Phys. Rev. Lett. **124**, 026401 (2020).